Severe Acute Respiratory Syndrome Coronavirus Evades Antiviral Signaling: Role of nsp1 and Rational Design of an Attenuated Strain[▽]

Marc G. Wathelet,[1]* Melissa Orr,[1] Matthew B. Frieman,[2] and Ralph S. Baric[2,3]

Department of Molecular and Cellular Physiology, University of Cincinnati College of Medicine, 231 Albert Sabin Way, Cincinnati, Ohio 45267-0576[1]; Departments of Epidemiology and Microbiology and Immunology[2] and Carolina Vaccine Institute,[3] University of North Carolina, Chapel Hill, North Carolina 27599-7435

The severe acute respiratory syndrome (SARS) epidemic was caused by the spread of a previously unrecognized infectious agent, the SARS-associated coronavirus (SARS-CoV). Here we show that SARS-CoV could inhibit both virus- and interferon (IFN)-dependent signaling, two key steps of the antiviral response. We mapped a strong inhibitory activity to SARS-CoV nonstructural protein 1 (nsp1) and show that expression of nsp1 significantly inhibited the activation of all three virus-dependent signaling pathways. We show that expression of nsp1 significantly inhibited IFN-dependent signaling by decreasing the phosphorylation levels of STAT1 while having little effect on those of STAT2, JAK1, and TYK2. We engineered an attenuated mutant of nsp1 in SARS-CoV through reverse genetics, and the resulting mutant virus was viable and replicated as efficiently as wild-type virus in cells with a defective IFN response. However, mutant virus replication was strongly attenuated in cells with an intact IFN response. Thus, nsp1 is likely a virulence factor that contributes to pathogenicity by favoring SARS-CoV replication.

Vertebrates have evolved sophisticated immunity mechanisms to manage infections by pathogens. The first line of defense is the innate immune response, which is initiated by the rapid recognition of pathogen-associated molecular patterns. In most cell types, viral RNA is sensed by RNA helicases (18) and triggers three signaling pathways, leading to the coordinated activation of the transcription factors ATF2/c-Jun, IRF3/IRF7, and NF-κB (25). In addition, double-stranded RNA and other viral determinants are recognized by Toll-like receptors expressed by specialized cells involved in the immune response. Signaling downstream of the Toll-like receptors involves various adaptor molecules and ultimately results in the activation of the same or a closely related set of transcription factors to those activated in the generic response (reviewed in reference 18).

Virus-activated transcription factors synergize to induce the production of a number of cytokines, including members of the type I interferon (IFN) family (which in humans comprises 14 IFN-α genes, 1 IFN-ω gene, and 1 IFN-β gene) and the type III IFN family (three human IFN-λ genes); inflammatory cytokines, such as interleukin-1 (IL-1), IL-6, IL-12, tumor necrosis factor alpha (TNF-α), and TNF-β; and chemokines, such as RANTES and IL-8. Together, these cytokines signal the occurrence of the infection and orchestrate the innate immune response directed against the invading virus (2, 33, 37).

Binding of type I or type III IFNs to their cognate receptors triggers a second wave of signaling, where phosphorylation and activation of the receptor-associated JAK1 and TYK2 kinases

result in the phosphorylation and activation of the transcription factors STAT1 and STAT2. Activated STAT1/STAT2 forms a complex with IRF9, termed ISGF3, which activates the transcription of a set of IFN-inducible genes by binding to their IFN-stimulated response elements (ISREs) (1, 33, 37).

The functional consequence of these two waves of signaling is the increased expression of IFN-inducible proteins that collectively inhibit the replication of a broad spectrum of viruses (33, 37). The importance of IFNs in vivo is underscored by viruses having evolved a wide variety of mechanisms to circumvent this antiviral response and by the dramatic increase in susceptibility to viral infection in mice where components of the IFN system have been inactivated (10, 14, 33, 46).

A previously unknown coronavirus, severe acute respiratory syndrome-associated coronavirus (SARS-CoV), has been isolated from patients with SARS (8, 20, 29) and fulfills Koch's postulates as the etiological cause of the SARS epidemic (9). SARS-CoV genome expression starts with the translation of two large replicative polyproteins, pp1a (486 kDa) and pp1a/b (790 kDa), which are encoded by the viral replicase gene, which contains two open reading frames (ORFs), ORFs 1a and 1b (Fig. 1D). Expression of the ORF 1b-encoded region of pp1a/b involves ribosomal frame shifting just upstream of the ORF 1a translation termination codon. The pp1a and pp1a/b polyproteins are processed by viral proteinases to yield the functional components of the replicase complex. The replicase mediates both replication and transcription of a set of subgenomic mRNAs for the expression of an additional eight genes (26, 31).

Precious little is known, however, about the interactions between the IFN system and SARS-CoV or other coronaviruses, although putative IFN antagonists have recently been identified through overexpression studies (17, 19). Here we show that while SARS-CoV is sensitive to the antiviral state

* Corresponding author. Mailing address: Department of Molecular and Cellular Physiology, University of Cincinnati College of Medicine, 231 Albert Sabin Way, Cincinnati, OH 45267-0576. Phone: (513) 558-4515. Fax: (513) 558-5738. E-mail: marc.wathelet@uc.edu.
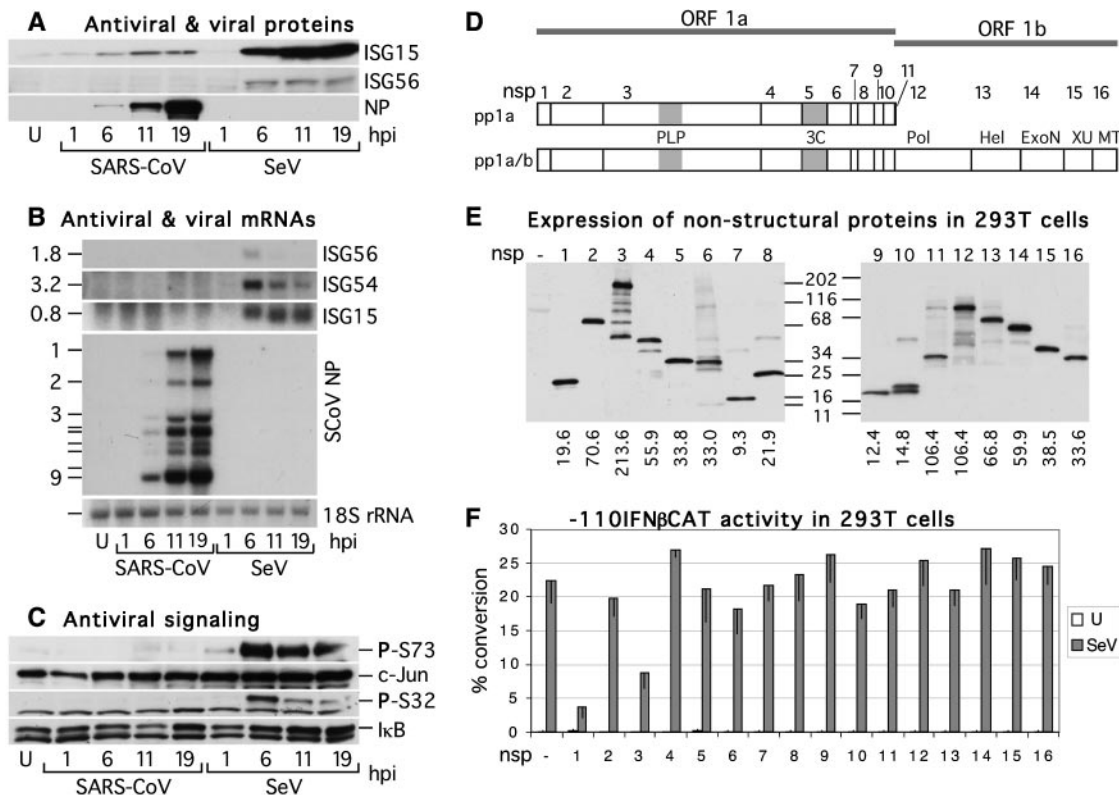
FIG. 1. (A) VeroE6 cells, uninfected (U) or infected for 1 h with WT SARS-CoV (MOI, 3) or SeV, were further incubated at 37°C. Protein extracts were harvested at the indicated times and analyzed by immunoblotting. Over the time course, the 15-kDa and 56-kDa proteins were more induced by SeV than by SARS-CoV (7.4- and 6.2-fold, respectively) (equal amounts of protein were verified by c-Jun and IκB levels [see panel C]). (B) RNAs from cells treated as described for panel A were analyzed by Northern blotting with the indicated probes. The signals for ISG54 and ISG15 mRNAs in SARS-CoV-infected samples are not bands but a smear that corresponds to low-level degradation of the much more intense rRNA signals that happen to also be detected by the ISG54 probe (28S rRNA) and the ISG15 probe (28S and 18S rRNAs). RNA sizes of the ISG bands are indicated on the left, in kb. Dashes mark the positions of the nine SARS-CoV RNAs. (C) Immunoblots as described for panel A were probed with anti-(phospho)-c-Jun or anti-(phospho)-IκB antibodies. (D) Structure of SARS-CoV replicase (see the text for more details). (E) Immunoblot analysis of extracts from 293T cells transfected with empty plasmid (−) or plasmids for the indicated Flag-nsp constructs. The predicted sizes of the nsps are indicated below the gel, in kDa. Different extract dilutions were used as follows: nsp1, 10×; nsp2, 150×; nsp3, 50×; nsp4, 100×; nsp5, 60×; nsp6, 10×; nsp7, 4×; nsp8, 4×; nsp9, 5×; nsp10, 30×; nsp11, 2×; nsp12, 2×; nsp13, 2×; nsp14, 200×; nsp15, 200×; and nsp16, 2×. (F) 293T cells transfected with empty plasmid (−) or plasmids for the indicated Flag-nsp constructs, together with −110IFNβCAT, were left uninfected (U) or infected with SeV for 18 h, and reporter activity was determined after normalization for transfection efficiency, not nsp expression levels.

established by IFN pretreatment, two critical aspects of the IFN response, virus- and IFN-dependent signaling, are both inhibited in SARS-CoV-infected cells. We demonstrate that SARS-CoV nsp1 mediates the inhibition of antiviral signaling, at least in part, and that an attenuating mutation in nsp1 decreases the ability of SARS-CoV to replicate in cells with an intact IFN response.

MATERIALS AND METHODS

Cell culture and viruses. VeroE6 cells are a clone of Vero cells, which are normal epithelial cells derived from African green monkey kidneys (ATCC CRL-1586). Calu-3 cells are tight junction-forming human epithelial lung cells derived from the pleural effusion of a lung adenocarcinoma (ATCC HTB-55). 293T cells are a simian virus 40 large T antigen-expressing highly transfectable derivative of 293 cells, which are derived from human embryonic kidney cells transformed with human adenovirus type 5. These cells were grown at 37°C in 5% CO$_2$ in Dulbecco's modified Eagle medium containing 10% fetal bovine serum, 50 U/ml penicillin, and 50 μg/ml streptomycin. Sendai virus (SeV; SPAFAS) was used at 25 hemagglutinating units/ml. Vesicular stomatitis virus (VSV; Indiana strain) was grown on VeroE6 cells, and the 50% tissue culture

infective dose was determined by limiting dilution and converted to PFU using Kärber's formula (one 50% tissue culture infective dose = 0.7 PFU).

All work with live SARS-CoV was performed in a biosafety cabinet in a biosafety level 3 (BSL3) laboratory by personnel dressed in Tyvek suits with full hoods, face shields, and double gloves and breathing through powered air-purifying respirators (BSL3+ standard). SARS-CoV (Urbani strain) was obtained from the CDC. Recombinant SARS-CoV strains, both wild type (WT) and m1, were derived as described previously (49). Plaque-purified SARS-CoVs were amplified on VeroE6 cells, and titers were determined by plaque assay or limiting dilution, as indicated. Second- and third-passage SARS-CoVs were used in all experiments, and the mutant virus was verified by sequencing.

Virus infections were performed in a small volume for 1 h, after which the inoculum was removed and the cells were washed once before further incubation. Because the initial infection was conducted at 37°C, the time of virus addition was taken as time zero. All virus titrations are averages for at least three independent experiments.

Cloning nsp cDNAs. The starting material was the Urbani strain of SARS-CoV 3200300841 at passage 3 in TRIzol LS reagent. Each cDNA was cloned by standard techniques (32) into a mammalian expression plasmid, pcDβAF$_3$m1, in frame with an N-terminal triple-Flag sequence (MDYKDHDGDYKDHDIDY KDHDE) or an N-terminal hemagglutinin tag (MAYPYDVPDYAS) and then fully sequenced. The nsp3 construct was somewhat unstable and was propagated

in *Escherichia coli* at room temperature; each preparation was fully sequenced. In the case of the nsp11 construct, the nsp11/nsp12 reading frames were cloned behind the Flag sequence so that nsp11 would be produced in the absence of frame shifting and nsp12 would be produced in its presence. In addition, an nsp12 construct was generated to have two nucleotide substitutions (underlined) that inactivate the "slippery" sequence required for frame shifting without altering the amino acid sequence and to have an insertion of an additional nucleotide (underlined and in bold) to produce the correct frame for nsp12 production (CGTTTTTAAACGGGTTT was changed to CGTT*C*TTGAAC*C*GGGTTT). For nsp1 m1 and m2, CTTCGTAAGAACGGTAATAAGGGA was mutated to CTTagtgagAACGGTAATAAGGGA for m1 and to CTTCGTAAGAACGGTagtgagGGA for m2 (mutations are shown in lowercase). All mutations were made by PCR, and the mutated region was fully sequenced.

Plasmids for H$_6$IRF3 and c-Jun have been described previously (40, 45). Plasmids for STAT1α (pcDβAMT-STAT1α) and STAT2 (pcDβAH$_6$STAT2) contain the coding region fused to an N-terminal Myc tag (MEQKLISEEDLN) and a hexahistidine tag, respectively. Plasmids for JAK1 (pRK-5-JAK1) and TYK2 (pRc/CMV-TYK2-VSV) were kind gifts of J. Ihle and S. Pelligrini, respectively. The plasmid for luciferase (*Photinus pyralis*) was generated by cloning the coding region into pcDβA. Reporters and the plasmid for Gal4-IRF7B have been described previously (45), and Gal4-p65 and Gal4-STAT2 were similarly constructed. All proteins were expressed from the cytomegalovirus (CMV) enhancer, except for the Gal4 fusions, which were expressed from the simian virus 40 enhancer.

Cell transfections and reporter assays. 293T cells (2.5×10^6) in 100-mm dishes were transfected by calcium phosphate coprecipitation (32) with 1 ml of a precipitate containing 5 μg reporter, 0 to 15 μg effector plasmid, 3 μg pCMV-lacZ, 2 μg pcDβA-luciferase, and pcDβA to a total of 25 μg for 18 h, trypsinized, aliquoted for further treatments, and harvested 2 days after transfection (transfection efficiency was routinely >95%, as determined by in situ *lacZ* staining).

Cell extracts were made with M-Per (Pierce). Chloramphenicol acetyltransferase (CAT), luciferase, and β-galactosidase activities were determined (32); CAT activity (computed as the percentage of conversion from unacetylated to monoacetylated chloramphenicol from phosphorimager data [% conversion = monoacetylated chloramphenicol/total chloramphenicol]), after normalization to the luciferase transfection efficiency control, was expressed in arbitrary units so that the relative strengths of reporters or activators could be estimated. Statistical significance was determined using a two-tailed *t* test on two sets of samples, assuming unequal variances; for the standard deviation, only the down line is shown in Fig. 1, 3, 4, and 5.

Expression of SeV proteins was not affected by nsp1 (not shown), as previously reported (17).

Immunoblot and Northern blot analyses. Cell extracts were analyzed by sodium dodecyl sulfate-polyacrylamide gel electrophoresis (SDS-PAGE) and immunoblotting as described previously (15). To ensure that equal amounts of protein were loaded into the gel, equal numbers of cells were seeded for each treatment and carefully harvested in the same volume of either M-Per (Pierce) or 2× SDS loading dye. Immunoblots with control antibodies as well as nonspecific bands with some antibodies confirmed equal loading for all immunoblots shown. We used the following commercial primary antibodies: rabbit polyclonal, anti-SARS-CoV NP (IMG-549; Imgenex), anti-c-Jun (9162; Cell Signaling), anti-phospho-Ser73-c-Jun (9164; Cell Signaling), anti-IκB (9242; Cell Signaling), anti-phospho-Ser32-IκB (9241; Cell Signaling), anti-IRF7 (sc-9083; Santa Cruz Biotechnology), anti-Gal4 antibody (sc-510; Santa Cruz Biotechnology), anti-STAT1 (sc-592; Santa Cruz Biotechnology), anti-phospho-Ser727-STAT1 (9177; Cell Signaling), anti-STAT2 (sc-22816 Santa Cruz Biotechnology), anti-phospho-Tyr690-STAT2 (4441; Cell Signaling), anti-Jak1 (3332; Cell Signaling), anti-phospho-Tyr1022/23-Jak1 (3331; Cell Signaling), anti-Tyk2 (ab5383; Abcam), anti-phospho-Tyr1054/55-Tyk2 (9321; Cell Signaling), anti-VSV G (Immunology Consultants Laboratory, Inc.), mouse monoclonal anti-phospho-Tyr701-STAT1 (sc-8394; Santa Cruz Biotechnology), and M2 (anti-Flag; Sigma) to detect Flag-tagged proteins. We also used rabbit polyclonal anti-UCRP (i.e., anti-ISG15; a kind gift of A. Haas), anti-ISG56 (a kind gift of G. Sen), anti-SARS-CoV nsp1, anti-SARS-CoV nsp3N, anti-SARS-CoV nsp3C (VU231, VU233, and VU235, respectively; kind gifts of M. R. Denison [30]), and the mouse monoclonal antibody SL-12 to detect IRF3 dimerization following deoxycholate-PAGE as described previously (48). The binding of these primary antibodies was detected with anti-mouse or anti-rabbit immunoglobulin–horseradish peroxidase conjugate as the secondary antibody (Promega). The chemiluminescence detection system was from Perkin-Elmer Life Sciences. RNAs were extracted with Tri-Reagent (Molecular Research), and Northern blot analysis of total RNA was performed using ISG15, ISG54, ISG56, and NP (nucleo-

tides 28,120 to 29,388) radioactive riboprobes exactly as described previously (44).

RESULTS

Virus-dependent signaling in SARS-CoV-infected cells. Virus infection leads to the induction of a set of cellular proteins unless the virus inhibits this antiviral response. SeV, a potent inducer of virus-dependent signaling, induced the 15- and 56-kDa proteins encoded by the virus- and IFN-inducible ISG15 and ISG56 genes. In contrast, induction of the ISG15 and ISG56 products was weaker at all time points in SARS-CoV-infected cells, where expression of SARS-CoV NP increased over the course of infection (Fig. 1A).

The weak expression of antiviral proteins in SARS-CoV-infected cells could be due to the inhibition of protein translation often observed during viral infections or to an inhibition at the RNA level. The ISG15, ISG54, and ISG56 mRNAs were undetectable in SARS-CoV-infected VeroE6 cells, while they were expressed in response to infection by SeV (Fig. 1B)(or by Newcastle disease virus ([44]). Expression of all SARS-CoV RNAs could be detected using an NP probe (Fig. 1B).

The undetectable expression of antiviral mRNAs in SARS-CoV-infected cells could be due to an inhibition of virus-dependent signaling. The transcriptional induction of ISG mRNAs by viruses depends on IRF3/IRF7, and activation of IRF3 is defective in SARS-CoV-infected cells (36). Induction of the IFN-β mRNA requires ATF2/c-Jun and NF-κB in addition to IRF3/IRF7. Phosphorylation of S73 in c-Jun was readily detectable after SeV infection but was very weak in SARS-CoV-infected cells. Similarly, phosphorylation of the NF-κB inhibitor IκB on S32 was undetectable in response to SARS-CoV but was robust in SeV-infected cells (Fig. 1C).

Thus, virus-dependent signaling appears to be weak in VeroE6 cells infected by SARS-CoV, in marked contrast to the response observed for SeV. We next focused on the nonstructural proteins carried by SARS-CoV as potential virulence factors because they are expressed early, before the generation of viral double-stranded RNA, which triggers antiviral signaling.

Expression of SARS-CoV replicase proteins in human cells. The SARS-CoV replicase polyproteins are predicted to be processed into 16 polypeptides, nsp1 to nsp16, by a 3C-like proteinase (3C) and a papain-like proteinase (35, 41) (Fig. 1D). 293T cells transfected with Flag-tagged nsp constructs produced proteins of the expected sizes, with wide variations in expression levels; e.g., nsp14 and -15 were expressed ~100-fold more than nsp12 and -16 were (Fig. 1E).

Expression of Flag-nsp3, which contains the papain-like proteinase activity, yielded a number of shorter polypeptides, some of which were also observed in SARS-CoV-infected cells (30). Expression of nsp4 is expected to produce a 56-kDa protein, but only a 38-kDa protein has been observed in SARS-CoV-infected cells (30). Nevertheless, we observed a protein of ~56 kDa in cells transfected with Flag-nsp4, but only when the cells were lysed in the presence of SDS, suggesting that nsp4 might be tightly associated with an insoluble cellular structure.

The nsp11 construct contained the sequence encoding nsp11 and -12, so both nsp11 and nsp12 were expected to be produced. To express nsp12 only, we introduced nucleotide sub-
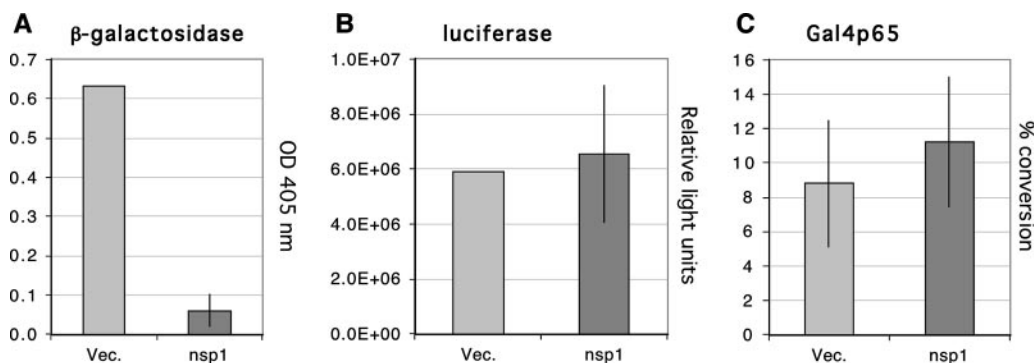
FIG. 2. 293T cells were transfected with empty vector (Vec.) or a vector for Flag-nsp1 expression (nsp1), together with different reporters and the CMV-*lacZ* and pcDβA-luciferase transfection efficiency controls (used in Fig. 1, 3, 4, and 8). (A) β-Galactosidase activity was assayed in a 150-μl reaction mix with *ortho*-nitrophenyl-β-galactopyranoside in a 96-well plate and read on an enzyme-linked immunosorbent assay reader at 405 nm every 5 min after the start of the reaction. Values in the linear range of the assay were normalized to the average (0.634) for cells transfected with empty vector, and nsp1 expression resulted in an average decrease to a value of 0.060, with a standard deviation of 0.040. (B) Luciferase activity was assayed in a 60-μl reaction mix by using a luciferase assay kit (Roche) and read in a Femtomaster FB12 instrument (Zylux). Values in the linear range of the assay were normalized to the average (5,899,000) for cells transfected with empty vector, and nsp1 expression resulted in an 11% increase, which was not statistically significant, to a value of 6,562,000 (standard deviation of 2,482,000). (C) 293T cells were transfected with empty vector (Vec.) or a vector for Flag-nsp1 expression (nsp1), together with the G5E1bCAT reporter, which contains five copies of the upstream activating sequence, a 17-mer binding site for Gal4, and a construct expressing the DNA-binding domain of Gal4 (amino acids 1 to 147) fused to the full-length coding region of the 65-kDa subunit of NF-κB (Gal4p65). CAT activity was assayed and normalized to luciferase activity. The average activity of Gal4p65 activating the G5E1bCAT reporter was increased 28% when nsp1 was coexpressed, but the increase was not statistically significant ($P = 0.28$).

stitutions that inactivate the "slippery" sequence required for frame shifting (41) without altering the amino acid sequence and inserted an additional nucleotide to produce the correct open reading frame for nsp12 production. Transfection of the Flag-nsp11 construct resulted in the expression of nsp12 through frame shifting, but with a lower yield than that of the Flag-nsp12 construct, as expected.

SARS-CoV nsp1 and nsp3 inhibit virus-dependent activation of the IFN-β promoter. SeV is a potent IFN inducer in human cells and has been used widely to characterize virus-dependent signaling and the IFN-β gene promoter (25). Infection by SeV of 293T cells transfected with the −110IFNβCAT reporter led to a strong increase in CAT activity (~225-fold) (Fig. 1F). We found that coexpression of most Flag-nsps had little effect on induction (<20%). However, coexpression of Flag-nsp1 or Flag-nsp3 each reduced induction of this promoter, by factors of ~6 ($P < 0.001$) and ~2.5 ($P = 0.001$), respectively. Expression of nsp1 also strongly affected one transfection efficiency control used, CMV-*lacZ*, making it unsuitable for experiments involving nsp1, but had no effect on another, pcDβA-luciferase, or on a CAT reporter driven by a constitutive activator (Fig. 2). Thus, experiments could be normalized for transfection efficiency by using luciferase activity, and effects on CAT reporters reflected signal transduction/promoter effects rather than a direct effect on expression of the CAT enzyme.

Expression from the IFN-β promoter depends on three *cis*-acting elements, PRDIV, P31, and PRDII, which in virus-infected cells are bound by the transcription factors ATF-2/c-Jun, IRF3/IRF7, and NF-κB, respectively (45). We next investigated how nsp1 and nsp3 inhibited expression of the IFN-β promoter by determining their effects on individual *cis*-acting elements and/or transcription factors.

SARS-CoV nsp1 and nsp3 inhibit activation of an NF-κB-dependent reporter. There was a strong increase in CAT activity in cells transfected with the NF-κB-dependent PRDIIx3CAT reporter and infected with SeV (~100-fold) or treated with TNF (~300-fold) (Fig. 3A). Coexpression of Flag-nsp3 resulted in a small decrease in the response to TNF that was not significant ($P = 0.07$) and an ~2.3-fold reduction in response to SeV that was significant ($P = 0.003$). Coexpression of Flag-nsp1 significantly decreased both TNF (~8.6-fold)- and SeV (~48-fold)-dependent activation of PRDIIx3CAT, indicating that nsp1 could inhibit the NF-κB pathway.

SARS-CoV nsp1 inhibits virus-dependent activation of IRF3 and IRF7. Virus-dependent phosphorylation of IRF3 and IRF7 leads to a conformational change that converts these latent cytoplasmic factors to active nuclear transcription factors targeting the P31 *cis*-acting element in the IFN-β promoter. Infection by SeV of cells transfected with P31x3CAT led to a strong increase in CAT activity (~40-fold) (Fig. 3B). Coexpression of Flag-nsp3 resulted in a small, statistically insignificant ($P = 0.14$) increase in the response of P31x3CAT to SeV. Coexpression of Flag-nsp1 strongly inhibited SeV-dependent activation of P31x3CAT (~29-fold; $P = 0.006$) (Fig. 3B). We next investigated the activation of IRF3 and IRF7. Cells were transfected with a plasmid directing the expression of IRF3 so that the signal from the fraction of cells that were untransfected would not obscure the inhibitory effect of nsp1, if any. Cotransfection of both IRF3 and Flag-nsp1 resulted in a strong decrease in virus-dependent dimerization of IRF3 compared to that in cells transfected with IRF3 alone, while nsp3 had no effect (Fig. 3C).

Activation of IRF7 independently of IRF3 was assessed using a Gal4-IRF7 fusion construct and a reporter driven by Gal4 binding sites, namely, G5E1bCAT. Infection with SeV resulted
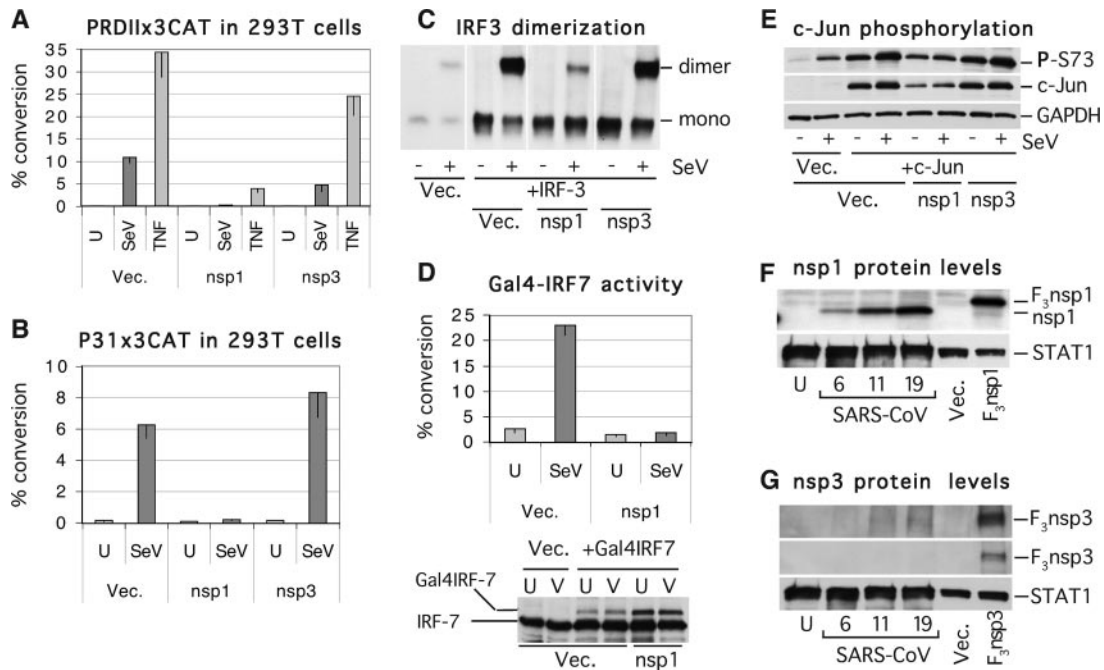
FIG. 3. (A) 293T cells transfected with empty vector (Vec.) or vector for nsp1 or nsp3, together with PRDIIx3CAT, were left uninfected (U), infected with SeV, or treated with 10 ng/ml of TNF for 18 h, and reporter activity was determined. (B) 293T cells transfected with empty vector (Vec.) or vector for nsp1 or nsp3, together with P31x3CAT, were left uninfected (U) or infected with SeV for 18 h, and reporter activity was determined. (C) 293T cells transfected with empty vector (Vec.) or vectors for expression of Flag-nsp1, Flag-nsp3, and/or H_6IRF3 were left uninfected (−) or infected with SeV (+) for 6 h, and extracts were analyzed by deoxycholate-PAGE and immunoblotting. (D) 293T cells transfected with Gal4-IRF7B, G5E1bCAT, and empty vector (Vec.) or a vector for nsp1 were left uninfected (U) or infected with SeV for 18 h, and reporter activity was determined. Extracts were also analyzed by immunoblotting with an anti-IRF7 antibody, which detects both Gal4-IRF7 and endogenous IRF7 (bottom). (E) 293T cells transfected with empty vector (Vec.) or vectors for nsp1, nsp3, and/or c-Jun were left uninfected (−) or infected with SeV (+) for 6 h, and expression and phosphorylation of c-Jun were determined by immunoblotting. GAPDH expression did not vary under these conditions. (F) VeroE6 cell extracts used for Fig. 1A and extracts of 293T cells transfected with empty vector (Vec.) or Flag-nsp1 were analyzed by immunoblotting with anti-nsp1 (VU231) (30) and anti-STAT1 antibodies. (G) VeroE6 cell extracts used for Fig. 1A and extracts of 293T cells transfected with empty vector (Vec.) or Flag-nsp3 were analyzed by immunoblotting with two anti-nsp3 antibodies (VU235 [top] and VU233 [middle], specific for the C and N termini, respectively [30]) and anti-STAT1 antibody [bottom].

in a robust induction of this reporter system (~8.5-fold) (Fig. 3D), as previously shown (45). Coexpression of Flag-nsp1 almost completely blocked this activation, while the expression level of Gal4-IRF7 itself was stimulated. In contrast, nsp1 had little effect on the activity of Gal4-p65 (Fig. 2C) or Gal4-STAT2 (see Fig. 5C). Thus, the virus-dependent activation of the P31 element and of both IRF3 and IRF7 was inhibited by coexpression of nsp1.

SARS-CoV nsp1 inhibits c-Jun expression and phosphorylation. The virus-dependent phosphorylation of c-Jun on S 73 by c-Jun N-terminal protein kinase can be assessed by immunoblotting. For cells transfected with empty vector only, phosphorylation of endogenous c-Jun on S73 was much stronger in cells infected with SeV than in uninfected cells, as expected. Cotransfection of c-Jun led to an increase in the c-Jun signal, but while SeV infection resulted in increased phosphorylation, a substantial basal phosphorylation was also detected. Coexpression of Flag-nsp3 had no discernible effects, but coexpression of Flag-nsp1 resulted in a decrease in c-Jun expression levels and suppressed virus-dependent phosphorylation (Fig. 3E).

Physiological expression levels of nsp1 and nsp3. Flag-nsp1 levels in transiently transfected 293T cells were comparable to the nsp1 levels observed in SARS-CoV-infected VeroE6 cells,

as determined by immunoblotting using an anti-nsp1 antibody (the nsp1 level in 293T cells was 98% of that in VeroE6 cells at 19 h postinfection [hpi] [Fig. 3F]). In contrast, the levels of Flag-nsp3 were substantially higher (3.4- to 16-fold) in 293T cells than those of nsp3 in SARS-CoV-infected cells, as determined by immunoblotting using anti-nsp3 antibodies directed against the N- and C-terminal parts of nsp3 (Fig. 3G) (nsp3 is barely detectable in infected cells, as reported previously [30]). Thus, expression of near physiological levels of SARS-CoV nsp1 in isolation substantially inhibited the virus-dependent pathways leading to activation of ATF2/c-Jun, IRF3/IRF7, and NF-κB, recapitulating the inhibition of signaling observed in SARS-CoV-infected cells. In contrast, SARS-CoV nsp3 inhibited only the NF-κB pathway, inhibited it relatively weakly only at supraphysiological levels, and was not further analyzed. Although speculative, the deubiquitinating activity of nsp3 (23) may account for its ability to inhibit the ubiquitination-dependent NF-κB pathway.

IFN-dependent response in SARS-CoV-infected cells. After virus-dependent signaling and induction of IFNs, the second step of the antiviral response is the IFN-dependent expression of a set of cellular proteins, which leads to the establishment of an antiviral state. VeroE6 cells were left uninfected or were infected with SARS-CoV for 9 h, after which the cells were
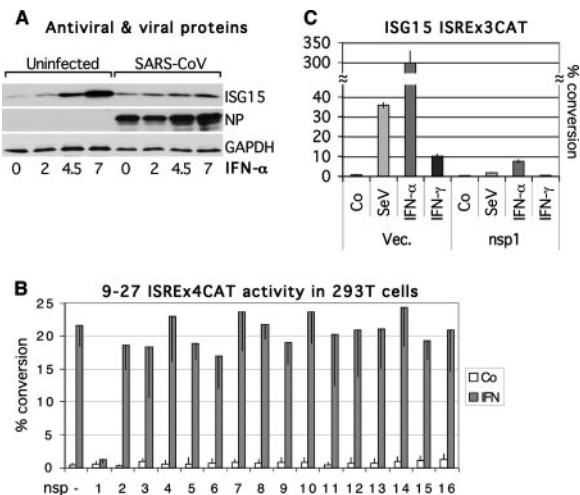
FIG. 4. (A) VeroE6 cells were left uninfected or were infected for 1 h with WT SARS-CoV (MOI, ~5) and further incubated for 8 h. IFN-α (2,000 U/ml) was then added for 2, 4.5, and 7 h before immunoblot analysis. (B) 293T cells transfected with 9-27 ISREx4CAT and empty vector (−) or Flag-nsp constructs were left untreated (Co) or treated with 500 U/ml of IFN-α for 18 h, and reporter activity was determined. (C) 293T cells transfected with ISG15 ISREx3CAT and empty vector (Vec.) or vector for nsp1 were left untreated (Co), infected with SeV, or treated with 500 U/ml of IFN-α or IFN-γ for 18 h, and reporter activity was determined.

FIG. 5. (A) 293T cells transfected with empty vector (−) or vectors for expression of nsp1 and/or STAT1α were treated with 2,000 U/ml of IFN-α or IFN-γ for 0, 10, 30, and 60 min, and extracts were analyzed by immunoblotting. (B) 293T cells transfected with empty vector (−) or vectors for nsp1 and/or STAT2 were treated with 2,000 U/ml of IFN-α for 0, 10, 30, and 60 min, and extracts were analyzed by immunoblotting. (C) 293T cells transfected with Gal4-STAT2, G5E1bCAT, and empty vector (Vec.) or a vector for nsp1 were left untreated (Co) or treated with 500 U/ml of IFN-α or IFN-γ for 18 h, and reporter activity was determined. Extracts were also analyzed by immunoblotting with an anti-STAT2 antibody, which detects the Gal4-STAT2 fusion and endogenous STAT2. Lanes 1 to 3, cells transfected with empty vector; lanes 4 to 6, cells transfected with Gal4-STAT2; lanes 7 to 9, cells transfected with Gal4-STAT2 and nsp1. Cells were left untreated (lanes 1, 4, and 7) or were treated for 18 h with 500 U/ml of IFN-α (lanes 2, 5, and 8) or IFN-γ (lanes 3, 6, and 9).

treated with IFN and further incubated for the indicated times (Fig. 4A). The ISG15 product was readily induced by IFN in uninfected cells, while IFN-dependent induction in SARS-CoV-infected cells was much reduced. Thus, induction of the virus- and IFN-inducible 15-kDa protein is defective both in response to virus and in response to IFN in SARS-CoV-infected cells.

SARS-CoV nsp1 inhibits activation of IFN-dependent reporters. We used CAT reporters driven by the ISRE of the 9-27 gene or the ISG15 gene to assess the effects of nsps on IFN-dependent signaling. Treatment of cells transfected with the 9-27ISREx4CAT reporter with IFN-α led to a strong increase in CAT activity (~44-fold) (Fig. 4B). Coexpression of most Flag-nsps had little effect (<16%) on induction of this reporter. However, coexpression of Flag-nsp1 inhibited the induction of 9-27ISREx4CAT by a factor of ~16 ($P < 0.001$). The 9-27 gene is part of a subset of IFN-inducible genes that respond only to IFN treatment, while there is another subset that also respond to virus infection (44), which we also tested. Infection with SeV or treatment with IFN-α or IFN-γ led to ~54-, ~450-, or ~15-fold activation of the ISG15 ISREx3CAT reporter, respectively. Coexpression of nsp1 resulted in an ~21-, ~40-, and ~29-fold inhibition of activation, respectively, by these stimuli (Fig. 4C). We next investigated how nsp1 inhibited the IFN-dependent activation of the ISRE by determining its effect on phosphorylation events in this pathway.

SARS-CoV nsp1 inhibits STAT1 phosphorylation. When cells are exposed to type I IFN, STAT1 becomes phosphorylated on Y701 and phosphorylation on S727 is further increased. The tyrosine phosphorylation is necessary for homo- or heterodimerization of STAT1, while the serine phosphorylation increases the transcriptional activity of STAT1. Cells
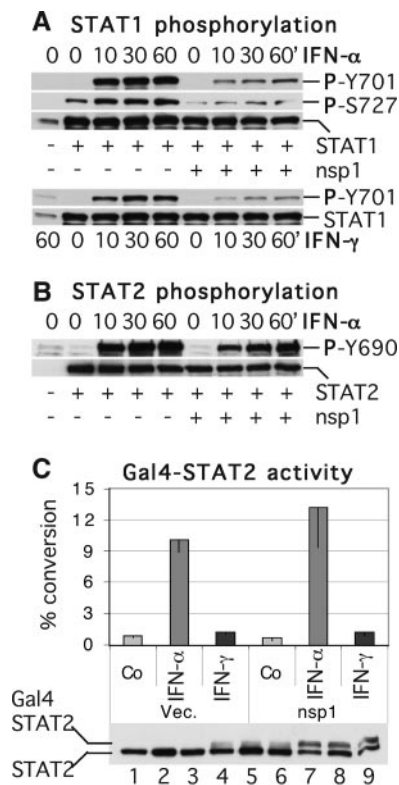
were transfected with a plasmid for STAT1α and treated with IFN-α or IFN-γ for 0, 10, 30, or 60 min (Fig. 5A). Both IFN-α and IFN-γ stimulated the levels of STAT1 phosphorylated on Y701, and coexpression of nsp1 decreased those levels while having no effect on the levels of the STAT1 protein. Similarly, phosphorylation of STAT1 on S727 was decreased by coexpression of nsp1.

SARS-CoV nsp1 only weakly inhibits STAT2 phosphorylation. When cells are exposed to type I IFN, STAT2 becomes phosphorylated on Y690, which allows it to heterodimerize with STAT1. IFN-α stimulated the levels of STAT2 phosphorylated on Y690, and nsp1 coexpression resulted in a small decrease in the levels of phospho-STAT2 and in the levels of the STAT2 protein (14% decrease after normalizing to the level of STAT2) (Fig. 5B). The activation of STAT2 independently of STAT1 was also assessed using Gal4-STAT2. Treatment with IFN-α resulted in a robust induction of the reporter
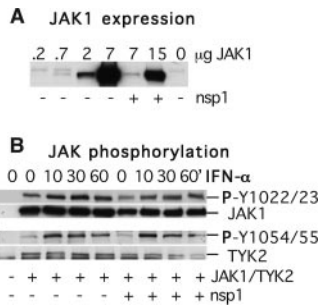
FIG. 6. (A) 293T cells were transfected with the indicated amounts of a JAK1 expression vector and with empty vector (−) or a vector for nsp1 (+), and the levels of JAK1 were determined by immunoblotting. (B) 293T cells transfected with empty vector (−) or vector for JAK1 or TYK2, with or without nsp1, were treated with 2,000 U/ml of IFN-α for 0, 10, 30, and 60 min, and extracts were analyzed by immunoblotting. To compensate for the effect of nsp1 on JAK1 levels, 10 μl of extracts transfected with 7 μg of JAK1 and 30 μl of extracts cotransfected with 15 μg of JAK1 and 15 μg of nsp1 were loaded in the gel.

FIG. 7. 293T cells transfected with empty vector (Vec.) or a vector for nsp1, together with pcDβA-eGFP, for 48 h were fixed, stained with PI in the presence of RNase A, and analyzed using flow cytometry to determine DNA content and the distribution of the cell population in the various phases of the cell cycle.

driven by Gal4 binding sites, i.e., G5E1bCAT (~12-fold) (Fig. 5C). Treatment with IFN-γ led to a modest induction (1.4-fold; $P = 0.006$). Expression of nsp1 led to a small, insignificant ($P = 0.14$) increase in IFN-α-dependent activation of Gal4-STAT2 and had no effect on IFN-γ-dependent activation. The expression levels of the Gal4-STAT2 fusion protein were stimulated by coexpression of nsp1, like the case for Gal4-IRF7. Thus, phosphorylation and activation of STAT2 were minimally affected by nsp1 expression.

SARS-CoV nsp1 does not inhibit JAK phosphorylation. Phosphorylation of STAT1 and STAT2 upon type I IFN treatment is effected by two JAK kinases associated with the type I IFN receptor, JAK1 and TYK2. Binding of IFN to its receptor leads to the phosphorylation of JAK1 on Y1022 and Y1023 and of TYK2 on Y1054 and Y1055, which can be detected with specific antibodies. Transient expression of JAK1 had a nonlinear dose response and was strongly inhibited by nsp1 (Fig. 6A). To assess JAK1 phosphorylation, different levels of JAK1 were transfected in the presence or absence of nsp1 and different amounts of extracts were used for immunoblot analysis so that the total amounts of JAK1 were comparable (Fig. 6B). IFN-dependent phosphorylation of both JAK1 and TYK2 was detected, and nsp1 had little or no effect on phosphorylation of either kinase when the total amount of each kinase was taken into account. Thus, it appears that expression of nsp1 resulted in substantially decreased levels of STAT1 phosphorylation on both Y701 and S727 and in a dramatic inhibition of JAK1 expression while having little effect on the phosphorylation levels of STAT2, JAK1, and TYK2.

Pleiotropic activities of nsp1. Besides inhibiting antiviral signaling, we found that nsp1 displayed multiple activities. We observed the following differences between 293T cells transfected with Flag-nsp1 and cells transfected with empty vector or other Flag-nsp constructs: (i) a significant decrease was observed in the total protein concentration of cell extracts (with, on average, an ~40% reduction 2 days after transfection); (ii) reduced metabolism was seen (as indicated by the pH of the culture medium); and (iii) when cells were cotransfected with a vector for expression of enhanced green fluorescent protein (EGFP), the number of fluorescent cells did not in-
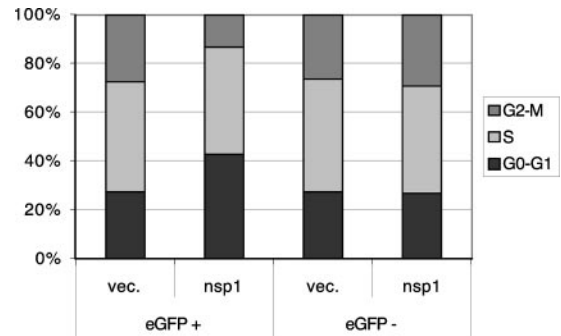
crease from the first day after transfection to the next only in the presence of Flag-nsp1 (not shown). To quantitatively document any effect of nsp1 on cell proliferation, transfected cells were fixed, stained with propidium iodide (PI) in the presence of RNase A, and analyzed using flow cytometry exactly as described previously (6). This method allows the determination of DNA content and provides an estimate of the distribution of a cell population in the various phases of the cell cycle. We found that with EGFP-positive cells, more cells were in the G_0/G_1 phase of the cycle at the expense of the G_2/M phase when nsp1 was present (Fig. 7). Gating on EGFP-negative cells (i.e., untransfected cells) showed the same cell cycle distribution as gating on EGFP-positive cells transfected with vector alone, as expected.

This inhibition of cell cycling did not lead to programmed cell death, as determined with unfixed cells stained with annexin V-allophycocyanin and PI, exactly as described previously (43). Annexin V staining detects the phospholipid phosphatidylserine, which is translocated from the inner leaflet of the plasma membrane to the outer leaflet in the early phase of apoptosis, and PI staining detects a compromised cellular membrane. These markers allow the identification of healthy, early apoptotic, late apoptotic/necrotic, and dead cells. We found that nsp1 expression decreased the percentage of apoptotic cells compared to that for cells transfected with empty vector (Table 1).

Moreover, expression of nsp1 led to decreased expression of some proteins (β-galactosidase, c-Jun, and JAK1) and increased expression of others (Gal4-IRF7 and Gal4-STAT2),

TABLE 1. Results of annexin V and PI staining[a]

Vector for cell transfection	% Stained cells			
	Annexin V− PI+ (dead)	Annexin V+ PI+ (late apoptosis/necrosis)	Annexin V− PI− (live)	Annexin V+ PI− (early apoptosis)
Empty vector	1.28	1.61	91.12	5.99
nsp1 vector	0.03	0.12	97.44	2.41

[a] 293T cells were transfected with empty vector or a vector for nsp1, together with pcDβA-eGFP, for 48 h, and unfixed cells were stained with annexin V-allophycocyanin and PI exactly as described previously (43).
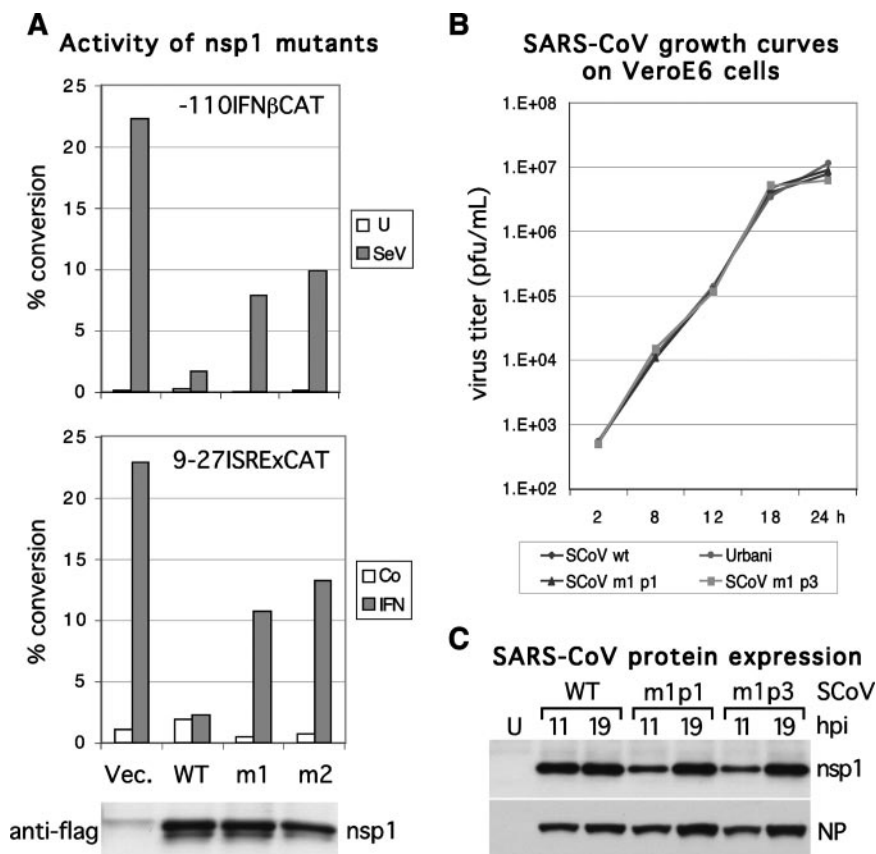
FIG. 8. (A) 293T cells were transfected with empty vector (Vec.) or vectors for WT or mutant Flag-nsp1 and reporters, as indicated. Cells transfected with −110IFNβCAT were left uninfected (U) or infected with SeV, and cells transfected with 9-27 ISREx4CAT were left untreated (Co) or treated with 500 U/ml of IFN-α for 18 h before reporter activity was determined. These extracts were also analyzed for nsp1 levels by immunoblotting (bottom). (B) Ninety percent confluent VeroE6 cells were infected with the indicated viruses at an MOI of ∼0.5. Supernatants were harvested at the indicated times postinfection, and their titers were determined by plaque assay. (C) VeroE6 cells were left uninfected (U) or were infected at an MOI of ∼3, and extracts were harvested at the indicated times for immunoblot analysis.

while most (e.g., luciferase, CAT, IRF3, STAT1, and TYK2) were not affected (Fig. 2, 3, 5, and 6).

Activity of SARS-CoV nsp1 mutants. To determine if nsp1 antagonist functions can be ablated, we introduced point mutations targeting amino acids predicted to be at the surface of the protein into nsp1 and, in this study, further characterized two among the mutants that had reduced activity, namely, m1 and m2. In nsp1 m1, R124 and K125 were replaced with S124 and E125, while in nsp1 m2, N128 and K129 were converted to S128 and E129. Cotransfection of mutant or WT nsp1 with a virus- or IFN-inducible reporter showed that the inhibitory effects of mutant nsp1 on the responses were much reduced compared to those of the WT (Fig. 8A) under conditions where the expression levels of the mutant nsp1s were close to those of WT nsp1 (bottom panel). In most experiments, however, nsp1 m1 and m2 were expressed at lower levels than the WT (∼2- to 3-fold lower) and had few remaining inhibitory effects on the response to virus (19 and 27% inhibition, respectively) or IFN (14 and 19% inhibition, respectively) at those levels. These mutations also had much less inhibitory activity towards CMV-*lacZ* expression (WT, m1, and m2 had 83, 24, and 17% inhibition, respectively).

The identification of inhibitory mutations in nsp1 makes it

possible to test the hypothesis that nsp1 is a virulence factor that allows SARS-CoV to evade the antiviral response. The nsp1 m1 mutation was introduced in the context of SARS-CoV by reverse genetics, and the growth curves for two SARS-CoV m1 plaques, p1 and p3, in VeroE6 cells were compared to those for the Urbani strain of SARS-CoV and recombinant WT SARS-CoV (Fig. 8B). The growth of SARS-CoV m1 p1 and p3 appeared to be unaffected compared to that of the WT strains, and sequencing confirmed mutation of only R124S and K125E in the recombinant viruses (data not shown). Expression of NP at 11 and 19 hpi was indistinguishable between the WT and m1 viruses, while the levels of nsp1 appeared to be decreased in the m1 viruses at the earlier time point (Fig. 8C).

Virus- and IFN-dependent responses in SARS-CoV m1-infected cells. The functional consequences of the nsp1 mutations introduced into SARS-CoV were investigated in VeroE6 cells and Calu-3 cells, which are lung epithelial cells with an intact IFN response (see below).

In VeroE6 cells, induction of ISG15 was much stronger with SARS-CoV m1 than with the WT at 12 and 18 hpi, while NP expression was not affected and expression of nsp1 was lower (Fig. 9A). In Calu-3 cells, induction of the ISG15 product was also stronger with SARS-CoV m1 than with the WT (3.9-
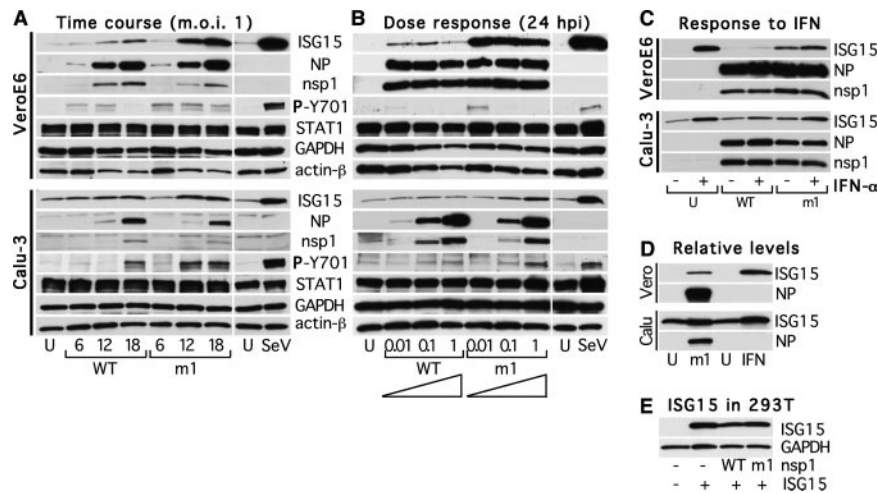
FIG. 9. (A) Immunoblot analysis of extracts from confluent VeroE6 or Calu-3 cells that were left uninfected (U) or infected with WT or m1p1 SARS-CoV (MOI, ~1) for the indicated times (h) or with SeV for 12 h [or 6 h in the case of anti-(phospho)-STAT1]. (B) Immunoblot analysis of extracts from confluent VeroE6 or Calu-3 cells that were left uninfected (U) or infected with WT or m1p1 SARS-CoV at the indicated MOIs (~0.01, 0.1, or 1) for 24 h or with SeV for 18 h [or 12 h in the case of anti-(phospho)-STAT1]. (C) Confluent VeroE6 or Calu-3 cells were left uninfected (U) or infected with WT or m1p1 SARS-CoV (MOI, ~0.1 for VeroE6 cells and ~1 for Calu-3 cells) for 24 h and treated with 500 U/ml IFN-α from 16 to 24 hpi (the last 8 h). Cell extracts were analyzed by immunoblotting. (D) Immunoblot analysis of extracts from the VeroE6 and Calu-3 cells used for panel C that were run side by side to directly compare the relative levels of expression of ISG15 is uninfected cells (U), cells infected with SARS-CoV ml (ml), and cells treated with IFN. (E) Immunoblot analysis of ISG15 ectopically expressed in 293T cells by transfection of a construct driven by the CMV promoter, pcDβA-hISG15, in the presence or absence of constructs for expression of nspl or ml, as indicated.

versus 2.8-fold), but the extent of the induction was partially masked by the rather high basal levels of the 15-kDa protein in these cells (Fig. 9D).

VeroE6 cells were also infected at three multiplicities of infection (MOI), namely, ~0.01, 0.1, and 1, for 24 h (Fig. 9B). At all doses, ISG15 was substantially more induced by SARS-CoV m1 than by the WT, but there were no differences in NP and nsp1 levels of expression, indicating that at these MOI, production of these viral proteins had reached steady-state levels by 24 hpi. The same experiment with Calu-3 cells again showed stronger induction of the ISG15 product by SARS-CoV m1 than that by the WT, with lower NP and nsp1 levels. The levels of STAT1 phosphorylation, which would reflect ongoing action by SARS-CoV-induced IFN, were also assessed. Phosphorylation of STAT1 on Y701 was consistently higher and was sustained longer in cells infected by SARS-CoV m1 than in those infected by the WT (Fig. 9A) (the sum of Y701 phosphorylation normalized to STAT1 levels at 6, 12, and 18 hpi was ~2.1-fold higher in response to the mutant virus for both cell lines). Thus, the decreased inhibitory activity of nsp1 m1 tested in isolation resulted in increased signaling and increased induction of a virus- and IFN-inducible gene product in the context of the virus.

The response to exogenous IFN in VeroE6 cells showed very little induction of ISG15 by IFN in WT SARS-CoV-infected cells over the levels achieved with the WT virus alone (Fig. 9C). In SARS-CoV m1-infected VeroE6 cells, IFN treatment led to an increase in the levels of the 15-kDa protein reached by infection alone, but without reaching the levels achieved by IFN treatment in uninfected cells. In Calu-3 cells infected by WT SARS-CoV, there was a small increase in ISG15 levels in response to IFN treatment (36% ± 12% of the increase observed in uninfected cells), and this increase was more sub-

stantial in SARS-CoV m1-infected cells (67% ± 2%) (Fig. 9C). Thus, the response to exogenous IFN was stronger in SARS-CoV m1-infected cells than in cells infected by the WT for both cell lines, but it remained partially inhibited. Expression of ISG15 from the CMV promoter was little affected by nsp1, suggesting that the data in Fig. 9A to D reflect effects on signaling rather than on ISG15 mRNA expression (Fig. 9E).

Antiviral activity against VSV. Before addressing the effectiveness of the antiviral state against SARS-CoVs, we challenged IFN-treated cells with VSV, which is very sensitive to IFN. At 18 hpi, supernatants were titrated (Fig. 10A) and cell extracts were analyzed by immunoblotting (Fig. 10B). While VeroE6 cells readily responded to IFN-α by inducing ISG15, the antiviral state against VSV was weak, with a substantial decrease in VSV G protein expression and VSV titers observed only with high doses of IFN (1,000 U/ml and higher) and with a net decrease in virus yield of only ~300-fold (from 7×10^7 to 2.2×10^5 PFU/ml). In contrast, strong reductions in titers and levels of VSV G were observed in Calu-3 cells with a much lower IFN dose (30 U/ml), and the virus yield decreased by a factor of ~20,000 (from 1×10^7 to 4.8×10^2 PFU/ml). Thus, a strong antiviral state can be established in Calu-3 cells, while the antiviral state in VeroE6 cells is weak and requires high doses of IFN.

Antiviral activity against SARS-CoVs. In VeroE6 cells, IFN pretreatment had no significant effect on replication of SARS-CoVs from 3 to 300 U/ml, and higher doses of IFN had a relatively modest effect (Fig. 10C and E), reducing virus replication by a factor of ~15 (from 1.6×10^6 to 1.1×10^5 PFU/ml). The difference in replication between the WT and mutant SARS-CoVs was very small (average, ~1.4-fold) and was not statistically significant. In Calu-3 cells, IFN pretreatment reduced SARS-CoV replication in a dose-dependent
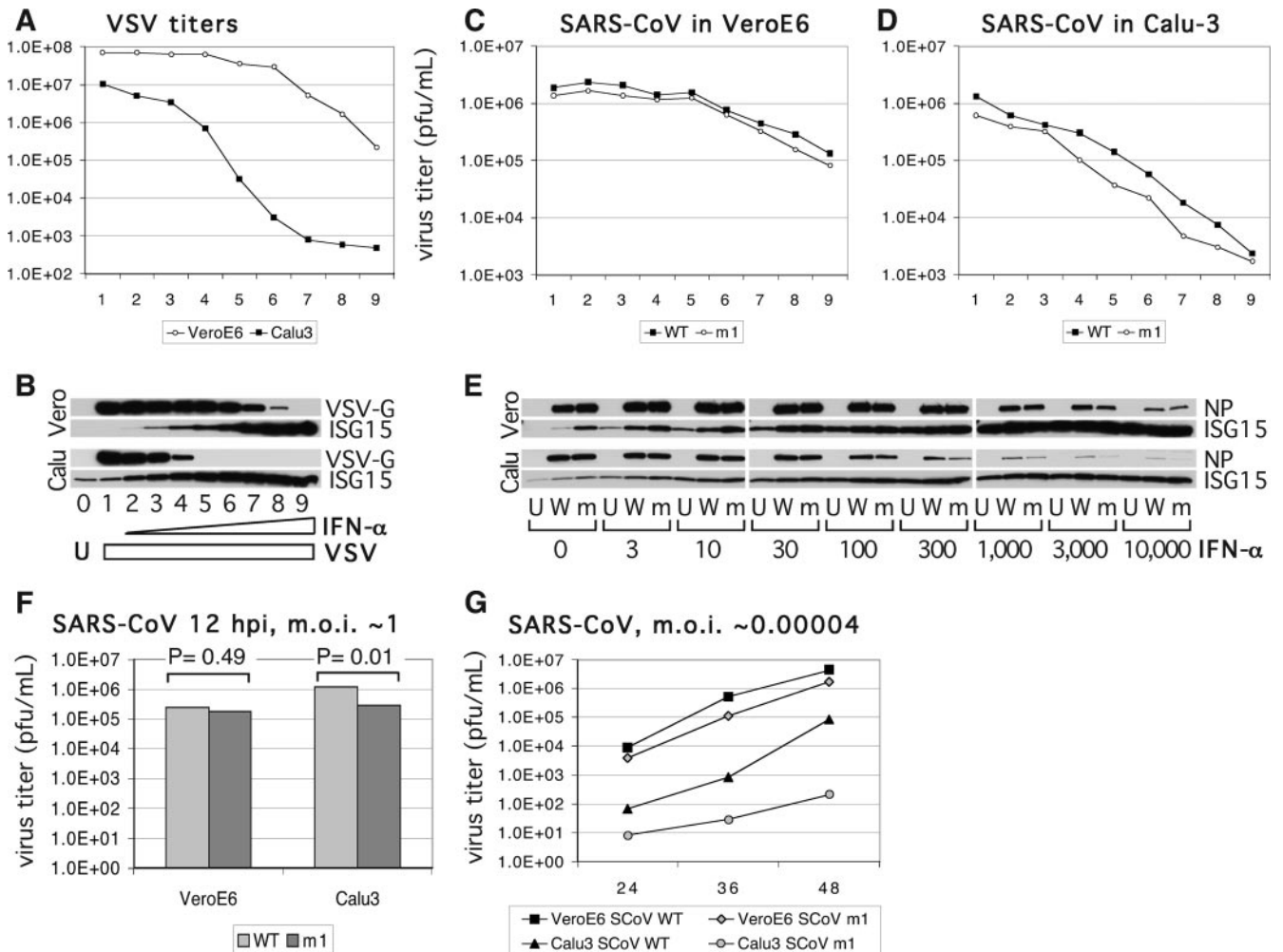
FIG. 10. (A and B) Confluent VeroE6 and Calu-3 cells were left untreated (lanes 0 and 1) or pretreated with increasing concentrations of IFN-α (lanes 2 to 9, 3, 10, 30, 100, 300, 1,000, 3,000, and 10,000 U/ml) for 24 h. Cells were left uninfected (U) or were infected with VSV for 1 h (MOI, ∼1), after which all cells were washed and further incubated for 17 h, when supernatants were titrated by limiting dilution (A) and cell extracts were analyzed by immunoblotting (B). (C to E) Confluent VeroE6 and Calu-3 cells were pretreated with increasing concentrations of IFN-α as described above, infected with WT SARS-CoV (W) or m1 (m) for 1 h (MOI, ∼1) or left uninfected (U), washed, and further incubated for 17 h, when supernatants were titrated by limiting dilution (C and D) and cell extracts were analyzed by immunoblotting (E). (F) Confluent VeroE6 and Calu-3 cells were infected with WT SARS-CoV and m1 (MOI, ∼1) for 12 h, and titers were determined by limiting dilution. (G) Confluent VeroE6 and Calu-3 cells were infected with WT SARS-CoV and m1 at a low MOI of ∼4 × 10⁻⁵, and supernatants were harvested at the indicated times (hpi) and titrated by limiting dilution. Each data point represents the average titer of 9 samples for VeroE6 cells with titers of at least 7×10^5 PFU/ml at 48 hpi or the average titer of 12 samples for Calu-3 cells (for Calu-3 cells, two WT SARS-CoV samples and six SARS-CoV m1 samples had undetectable levels of virus, i.e., <4.4 PFU/ml).

manner (Fig. 10D and E), decreasing it as much as ∼560-fold for the WT and ∼360-fold for m1. The average difference in replication titers between the WT and mutant viruses was small (∼2.4-fold) and presumably reflects the higher induction of IFN and other antiviral proteins by the mutant virus. Thus, IFN established an effective antiviral state against both viruses in response to IFN in Calu-3 cells but not in VeroE6 cells.

Attenuation of SARS-CoV m1 in cells with an intact IFN response. We next investigated the functional consequences of increased signaling on viral replication. Under conditions that minimize the impact of the IFN response (short replication time [12 h] and an MOI of ∼1), there was no significant effect of the nsp1 mutation on SARS-CoV replication in cells with a defective IFN response (Fig. 10F, VeroE6).

However, under conditions that mimic a natural infection, i.e., a low MOI, longer incubation times, and an intact IFN response, there was a drastic difference in replication between the nsp1 mutant SARS-CoV and the WT (Fig. 10G, Calu-3). Thus, SARS-CoV m1 titers were lower than WT titers by factors of ∼8, 29, and 390 at 24, 36, and 48 hpi, respectively, in Calu-3 cells. In contrast, in VeroE6 cells under the same conditions, the SARS-CoV m1 titers were lower than WT titers by factors of only ∼2.3, 4.6, and 2.7 at 24, 36, and 48 hpi, respectively (Fig. 10G, VeroE6).

WT SARS-CoV's ability to weakly activate antiviral signaling had an impact on its replication in cells with an intact IFN response. This was manifested by reduced titers in Calu-3 cells compared to those in VeroE6 cells when cells were infected at

a low MOI. (as much as ~600-fold at 36 hpi for WT SARS-CoV) (Fig. 10G). Thus, the sensitivity of SARS-CoV to the antiviral effects of IFN makes inhibition of antiviral signaling necessary for efficient replication, and this inhibition of signaling is mediated, at least in part, by nsp1.

DISCUSSION

SARS-CoV is sensitive to the antiviral state induced by type I IFNs, both in vitro (5, 38, 51; this study) and in vivo (13), prompting us to test the hypothesis that SARS-CoV inhibits IFN production and/or IFN-dependent signaling. Here we show that SARS-CoV can inhibit both virus- and IFN-dependent signaling, two key steps of the antiviral response. Using a transfection-based screen, which might not be as sensitive as screens based on heterologous viral expression (19) because several proteins were expressed at low levels (Fig. 1E), we identified nsp1 and nsp3 as potential IFN antagonists. However, only nsp1 inhibited antiviral signaling when expressed in isolation at physiological levels. We found that nsp1 by itself recapitulated the inhibition of signaling observed in infected cells and that the signaling inhibition in SARS-CoV-infected cells was mediated, at least in part, through nsp1.

Virus-dependent signaling. IFN-β induction has been shown to be defective in SARS-CoV-infected cells (4, 36, 52). Here we show that all three virus-dependent pathways were only weakly activated by SARS-CoV compared to their activation by SeV. SARS-CoV-dependent phosphorylation of c-Jun and IκB was very weak, as was induction of ISG15 (Fig. 1). ISG15 induction depends on IRF3/IRF7 activation, and dimerization of IRF3 was not detected in SARS-CoV-infected cells (36). Expression of nsp1 in isolation also inhibited the three virus-dependent pathways, namely, SeV-dependent activation of (i) an NF-κB-dependent reporter, (ii) IRF3 and IRF7, and (iii) c-Jun (Fig. 3). Introduction of a mutation that decreased the inhibitory activity of nsp1 in the context of SARS-CoV resulted in an increased production and action of IFN, as determined by STAT1 phosphorylation, and an enhanced expression of ISG15 compared to those induced by the WT virus (Fig. 9). Thus, SARS-CoV inhibits all virus-dependent pathways, at least in part, through expression of nsp1.

IFN-dependent signaling. Induction of ISG15 by IFN was weak in SARS-CoV-infected cells compared to that in uninfected cells, and expression of WT but not mutant nsp1 substantially inhibited IFN-dependent reporters. nsp1 specifically decreased the phosphorylation levels of STAT1 while having little effect on STAT2, JAK1, and TYK2 phosphorylation (Fig. 5 and 6). Accordingly, induction of ISG15 by IFN in cells infected with SARS-CoV m1 was stronger than that in cells infected with WT virus (Fig. 9). Thus, SARS-CoV inhibits IFN-dependent signaling, at least in part, through expression of nsp1 and specific inhibition of STAT1 phosphorylation.

Inhibition of cell cycling. We found that nsp1 inhibited cellular proliferation and progression through the cell cycle without affecting cell viability (Fig. 7; Table 1). The ortholog of nsp1 in mouse hepatitis coronavirus, p28, has also been shown to arrest the cell cycle in the G_0/G_1 phase (3), and we have observed that p28 inhibits antiviral signaling, too, although less efficiently than SARS-CoV nsp1 (M. G. Wathelet, unpublished data). Thus, nsp1 and other SARS-CoV proteins, e.g., NP and

ORF7a (39, 50), could contribute to the inhibition of cell proliferation observed in SARS-CoV-infected cells (27). This inhibition of cell cycle progression might impact the recovery from lung injury, as alveolar repair depends on type II alveolar epithelial cell proliferation to replace, after differentiation, the fragile type I alveolar epithelial cells (12).

SARS-CoV nsp1 mechanism of action. Expression by transient transfection of several genes, i.e., those encoding LacZ, c-Jun, and JAK1, under the control of the CMV enhancer was inhibited by nsp1. However, the expression of other genes under the control of that enhancer was not affected by nsp1 (e.g., the luciferase, IRF3, STAT1, and TYK2 genes), suggesting that nsp1 acted at the posttranscriptional level (Fig. 2, 3, 5, and 6). Recently, SARS-CoV nsp1 was shown to suppress *lacZ* and luciferase expression through mRNA degradation (17). Although *lacZ* mRNA degradation caused by nsp1 expression is consistent with our data, we did not observe a decrease in luciferase activity in cells expressing nsp1 (Fig. 2B). It is possible that sequences flanking the luciferase coding region are the targets of nsp1 and that they differ in the two studies. Our observation that the expression of a number of proteins was either not affected or stimulated by nsp1 indicates that nsp1 does not promote a general gene expression shutoff through host mRNA degradation. In addition, several chemokine mRNAs were recently reported to be induced by expression of nsp1 alone, possibly through nuclear translocation of p65 (21). This contrasts with our observations, with different cell lines, that phosphorylation of IκB was blocked in SARS-CoV-infected cells and that nsp1 inhibited the activation of an NF-κB-dependent reporter by either SeV or TNF (Fig. 1C and 3A); further studies are needed to resolve this issue.

Kamitani and colleagues also reported that IRF3 dimerization is not affected by nsp1 expression, in contrast to our observations (Fig. 3C) and to the report that IRF3 fails to dimerize in SARS-CoV-infected cells (36). The inhibition of IRF3 dimerization by nsp1 is consistent with the inhibition of the P31x3CAT reporter and the inhibition of Gal4-IRF7 (Fig. 2). A difference between the experimental procedures might account for the discrepancy: we cotransfected 293T cells with a plasmid directing the expression of IRF3 so that the signal from the fraction of cells that were untransfected or inefficiently transfected would not obscure the inhibitory effect of nsp1, while Kamitani and colleagues did not (17).

Glyceraldehyde-3-phosphate dehydrogenase (GAPDH) and β-actin mRNAs were identified as cellular mRNAs whose levels are decreased in cells transfected by nsp1 or infected by SARS-CoV (17). We observed a time- and dose-dependent decrease in the levels of both GAPDH and β-actin proteins in VeroE6 cells infected by SARS-CoV, but not in Calu-3 cells (Fig. 4A and 9). As noted above, nsp1 m1 is attenuated not only for inhibition of signaling but also for inhibition of *lacZ* expression. Nevertheless, there was no obvious difference between WT and mutant viruses for expression of these two cellular proteins (Fig. 9A and B). While the biological significance of lower expression of GAPDH and β-actin in response to SARS-CoV replication is unclear, we have identified JAK1 as a target of nsp1, and decreased expression of JAK1 could account for the inhibition of STAT1 phosphorylation (Fig. 5 and 6).

Several mechanisms, which are not necessarily mutually ex-

clusive, could account for nsp1's multiple activities. (i) nsp1 could destabilize a specific set of mRNAs directly or by increasing the activity or modifying the specificity of an endogenous nuclease. This mechanism might account not only for the reduced expression of a number of proteins but also for the observed defects in signaling if some of the mRNAs encoding key pathway components, such as JAK1, happen to be destabilized by nsp1. (ii) nsp1 could target the activity of one or a few proteins involved in signaling. This mechanism might account not only for the signaling inhibition but also for the destabilization of a specific set of mRNAs because mRNA stability can be controlled by signaling events. (iii) nsp1 could have independent activities, with one affecting mRNA stability and the other affecting signaling. Clearly, further studies are required to determine exactly how nsp1 exerts its effects.

SARS-CoV replication in IFN-sensitive cells. The SARS-CoV receptor is expressed on ciliated tracheobronchial epithelial cells, which can be infected productively by SARS-CoV in vivo (Wathelet, unpublished data), in vitro, and ex vivo, with entry and release through the apical domain and with cytopathic effects (34). Calu-3 cells are human lung epithelial cells from a bronchial adenocarcinoma that form a monolayer with tight junctions. They can be infected by SARS-CoV with cytopathic effects, with virus entry and release primarily through the apical domain (42). These properties of Calu-3 cells, their ease of propagation, and their sensitivity to IFN (this study) make them a very useful and relevant model for studying SARS-CoV in vitro.

Even though WT SARS-CoV activated antiviral signaling only very weakly (Fig. 1 and 9), this ability had an impact on its replication in cells with an intact IFN response. Thus, when cells were infected under conditions that maximized the IFN response, WT SARS-CoV replicated much more slowly in Calu-3 cells than in VeroE6 cells (8.5×10^2 PFU/ml in Calu3 cells versus 5.3×10^5 PFU/ml in VeroE6 cells, a 2.8-log difference, at 36 hpi) (Fig. 10G). This slower replication in Calu-3 cells is not due to an intrinsically lower rate of replication of SARS-CoV in these cells. When cells were infected under conditions that minimized the IFN response, SARS-CoV production in Calu-3 cells (1.2×10^6 PFU/ml) compared favorably with the yield obtained from VeroE6 cells (2.5×10^5 PFU/ml) (Fig. 10F). Therefore, the slower replication at a low MOI can only be explained by an extrinsic factor released by the infected cells, i.e., by secreted IFN, which has had the time to act on uninfected cells and protect them from subsequent infection by the virus.

Under conditions that mimic natural infection, there was a drastic difference in the growth kinetics of SARS-CoV m1 compared to that of the WT in Calu-3 cells (2.6 log at 48 hpi) (Fig. 10G). This difference is comparable to that observed for influenza virus when NS1 is mutated (1.4 log at 48 hpi) (7) or deleted (2.6 log at 48 hpi) (11). The difference in replication between WT and mutant SARS-CoV is fully consistent with the increased virus- and IFN-dependent signaling observed in cells infected by the mutant virus (Fig. 9) and with the IFN dose dependence in establishing an antiviral state in Calu-3 cells (Fig. 10D and E). In contrast, the difference in replication of the two strains was minimal in VeroE6 cells under these conditions (Fig. 10G). VeroE6 cells appear to be largely resistant to the establishment of an antiviral state in response to

IFN, and this is not due to a defect in signaling, as the induction of ISG15 was robust (Fig. 10A to E). Rather, expression of protein kinase R, a key antiviral enzyme (33, 37), is attenuated in VeroE6 cells, in part due to aberrant splicing (28). The difference between the two strains was also minimal in Calu-3 cells infected at a high MOI after 12 h (Fig. 10F), because under these conditions there is not enough time for the full establishment of an antiviral state.

Another manifestation of this phenomenon was observed when cells were infected at different MOIs (Fig. 9B). In VeroE6 cells, replication was unimpeded by IFN, and by 24 hpi, the maximum steady-state levels of NP and nsp1 had been reached for all MOIs tested. In contrast, replication at lower multiplicities was slowed in Calu-3 cells, and the effect was more marked with the mutant virus, implicating IFN production and action in this effect.

While SARS-CoV is not as sensitive to the antiviral state as VSV is (Fig. 10), its sensitivity to the antiviral effects of IFN makes inhibition of antiviral signaling necessary for efficient replication. When a mutation in nsp1 that decreased its ability to inhibit signaling was engineered into SARS-CoV, the replication of the resulting virus was attenuated under conditions where the IFN response can take place, as hypothesized. The difference between replication of WT SARS-CoV in VeroE6 cells and that of SARS-CoV m1 in Calu-3 cells reflects the total impact of the IFN response, with an ~20,000-fold decrease in titer at 36 and 48 hpi (Fig. 10G).

We concluded that nsp1 is a virulence factor that allows SARS-CoV to evade the IFN response in cell culture by inhibiting, directly and/or indirectly, the expression of virus- and IFN-inducible proteins involved in the antiviral response to SARS-CoV, based on the following four key findings: (i) virus- and IFN-dependent signaling is inhibited in SARS-CoV-infected cells, (ii) nsp1 expressed in isolation can inhibit virus- and IFN-dependent signaling, (iii) virus- and IFN-dependent signaling is higher in cells infected with mutant SARS-CoV than in those infected with WT virus, and (iv) SARS-CoV with an attenuating mutation in nsp1 replicates normally in cells with a defective IFN response and replicates much less effectively than WT virus in cells with an intact IFN response, but only under conditions that allow the IFN response time to develop.

Viruses have evolved a variety of mechanisms to evade the IFN response. Some viruses directly antagonize specific components of virus-dependent signaling, specific components of IFN-dependent signaling, or specific components of IFN effector pathways. In addition, some viruses indirectly antagonize the antiviral response by inhibiting general mechanisms of host cell gene expression. While such inhibition is nonspecific, it has been demonstrated that it is the indirect inhibition of the IFN response that is biologically significant. Moreover, some viruses evade the IFN response by a combination of direct and indirect mechanisms (reviewed in references 10, 14, 22, 33, 46, and 47 and in references therein). Here we show that SARS-CoV could evade the IFN response directly by inhibiting antiviral signaling and/or indirectly by affecting mRNA stability.

Another recent study identified proteins expressed from SARS-CoV subgenomic mRNAs as IFN antagonists when overexpressed in heterologous systems (19), but the effect of inactivating these proteins on SARS-CoV replication in IFN-

sensitive cells remains to be determined. The presence of multiple IFN antagonists in the SARS-CoV genome is intriguing but not unique (10, 14, 22, 33, 46, 47). It underscores the importance of evading the IFN response, and multiple antagonists may favor replication of this virus in different cell types and different species.

Pathophysiological relevance of our observations. The importance of IFN in controlling the replication of SARS-CoV is underscored by the worsening of symptoms in mice with STAT1 inactivation (16). The observation that SARS patients appeared to benefit from IFN treatment (24) suggests that the levels of IFN naturally produced in vivo are suboptimal, which is consistent with our observation that SARS-CoV and nsp1 inhibited IFN production. Prophylactic treatment of macaques with IFN reduces viral replication and pulmonary damage, while postexposure treatment yields intermediary results (13). Treatment of SARS patients with IFN would be expected to have little effect on replication in infected cells because of inhibition of IFN-dependent signaling but to effectively protect other cells from subsequent infection. Thus, our findings strengthen the rationale for using IFN to treat SARS patients.

REFERENCES

1. **Ank, N., H. West, C. Bartholdy, K. Eriksson, A. R. Thomsen, and S. R. Paludan.** 2006. Lambda interferon (IFN-λ), a type III IFN, is induced by viruses and IFNs and displays potent antiviral activity against select virus infections in vivo. J. Virol. **80:**4501–4509.
2. **Bogdan, C.** 2000. The function of type I interferons in antimicrobial immunity. Curr. Opin. Immunol. **12:**419–424.
3. **Chen, C. J., K. Sugiyama, H. Kubo, C. Huang, and S. Makino.** 2004. Murine coronavirus nonstructural protein p28 arrests cell cycle in G_0/G_1 phase. J. Virol. **78:**10410–10419.
4. **Cheung, C. Y., L. L. Poon, I. H. Ng, W. Luk, S. F. Sia, M. H. Wu, K. H. Chan, K. Y. Yuen, S. Gordon, Y. Guan, and J. S. Peiris.** 2005. Cytokine responses in severe acute respiratory syndrome coronavirus-infected macrophages in vitro: possible relevance to pathogenesis. J. Virol. **79:**7819–7826.
5. **Cinatl, J., B. Morgenstern, G. Bauer, P. Chandra, H. Rabenau, and H. W. Doerr.** 2003. Treatment of SARS with human interferons. Lancet **362:**293–294.
6. **Darzynkiewicz, Z., and G. Juan.** 1997. DNA content measurement for DNA ploidy and cell cycle analysis, p. 7.5.1–7.5.24. *In* J. P. Robinson et al. (ed.), Current protocols in cytometry. John Wiley & Sons, Inc., New York, NY.
7. **Donelan, N. R., C. F. Basler, and A. Garcia-Sastre.** 2003. A recombinant influenza A virus expressing an RNA-binding-defective NS1 protein induces high levels of beta interferon and is attenuated in mice. J. Virol. **77:**13257–13266.
8. **Drosten, C., S. Gunther, W. Preiser, S. van der Werf, H. R. Brodt, S. Becker, H. Rabenau, M. Panning, L. Kolesnikova, R. A. Fouchier, A. Berger, A. M. Burguiere, J. Cinatl, M. Eickmann, N. Escriou, K. Grywna, S. Kramme, J. C. Manuguerra, S. Muller, V. Rickerts, M. Sturmer, S. Vieth, H. D. Klenk, A. D. Osterhaus, H. Schmitz, and H. W. Doerr.** 2003. Identification of a novel coronavirus in patients with severe acute respiratory syndrome. N. Engl. J. Med. **348:**1967–1976.
9. **Fouchier, R. A., T. Kuiken, M. Schutten, G. van Amerongen, G. J. van Doornum, B. G. van den Hoogen, M. Peiris, W. Lim, K. Stohr, and A. D. Osterhaus.** 2003. Aetiology: Koch's postulates fulfilled for SARS virus. Nature **423:**240.
10. **Garcia-Sastre, A.** 2002. Mechanisms of inhibition of the host interferon alpha/beta-mediated antiviral responses by viruses. Microbes Infect. **4:**647–655.
11. **Garcia-Sastre, A., A. Egorov, D. Matassov, S. Brandt, D. E. Levy, J. E. Durbin, P. Palese, and T. Muster.** 1998. Influenza A virus lacking the NS1 gene replicates in interferon-deficient systems. Virology **252:**324–330.
12. **Geiser, T.** 2003. Mechanisms of alveolar epithelial repair in acute lung injury—a translational approach. Swiss Med. Wkly. **133:**586–590.
13. **Haagmans, B. L., T. Kuiken, B. E. Martina, R. A. Fouchier, G. F. Rimmelzwaan, G. van Amerongen, D. van Riel, T. de Jong, S. Itamura, K. H. Chan, M. Tashiro, and A. D. Osterhaus.** 2004. Pegylated interferon-alpha protects type 1 pneumocytes against SARS coronavirus infection in macaques. Nat. Med. **10:**290–293.
14. **Haller, O., G. Kochs, and F. Weber.** 2006. The interferon response circuit: induction and suppression by pathogenic viruses. Virology **344:**119–130.
15. **Harlow, E., and D. Lane.** 1988. Antibodies: a laboratory manual. Cold Spring Harbor Press, Cold Spring Harbor, NY.
16. **Hogan, R. J., G. Gao, T. Rowe, P. Bell, D. Flieder, J. Paragas, G. P. Kobinger, N. A. Wivel, R. G. Crystal, J. Boyer, H. Feldmann, T. G. Voss, and J. M. Wilson.** 2004. Resolution of primary severe acute respiratory syndrome-associated coronavirus infection requires Stat1. J. Virol. **78:**11416–11421.
17. **Kamitani, W., K. Narayanan, C. Huang, T. Lokugamage, T. Ikegami, N. Ito, H. Kubo, and S. Makino.** 2006. Severe acute respiratory syndrome coronavirus nsp1 protein suppresses host gene expression by promoting host mRNA degradation. Proc. Natl. Acad. Sci. USA **103:**12885–12890.
18. **Kawai, T., and S. Akira.** 2006. Innate immune recognition of viral infection. Nat. Immunol. **7:**131–137.
19. **Kopecky-Bromberg, S. A., L. Martinez-Sobrido, M. Frieman, R. A. Baric, and P. Palese.** 2007. Severe acute respiratory syndrome coronavirus open reading frame (ORF) 3b, ORF 6, and nucleocapsid proteins function as interferon antagonists. J. Virol. **81:**548–557.
20. **Ksiazek, T. G., D. Erdman, C. S. Goldsmith, S. R. Zaki, T. Peret, S. Emery, S. Tong, C. Urbani, J. A. Comer, W. Lim, P. E. Rollin, S. F. Dowell, A. E. Ling, C. D. Humphrey, W. J. Shieh, J. Guarner, C. D. Paddock, P. Rota, B. Fields, J. DeRisi, J. Y. Yang, N. Cox, J. M. Hughes, J. W. LeDuc, W. J. Bellini, and L. J. Anderson.** 2003. A novel coronavirus associated with severe acute respiratory syndrome. N. Engl. J. Med. **348:**1953–1966.
21. **Law, A. H., D. C. Lee, B. K. Cheung, H. C. Yim, and A. S. Lau.** 2007. Role for nonstructural protein 1 of severe acute respiratory syndrome coronavirus in chemokine dysregulation. J. Virol. **81:**416–422.
22. **Levy, D. E., and A. Garcia-Sastre.** 2001. The virus battles: IFN induction of the antiviral state and mechanisms of viral evasion. Cytokine Growth Factor Rev. **12:**143–156.
23. **Lindner, H. A., N. Fotouhi-Ardakani, V. Lytvyn, P. Lachance, T. Sulea, and R. Menard.** 2005. The papain-like protease from the severe acute respiratory syndrome coronavirus is a deubiquitinating enzyme. J. Virol. **79:**15199–15208.
24. **Loutfy, M. R., L. M. Blatt, K. A. Siminovitch, S. Ward, B. Wolff, H. Lho, D. H. Pham, E. A. LaMere, M. Chang, K. C. Kain, G. A. Farcas, P. Ferguson, M. Latchford, G. Levy, J. W. Dennis, E. K. Lai, and E. N. Fish.** 2003. Interferon alfacon-1 plus corticosteroids in severe acute respiratory syndrome: a preliminary study. JAMA **290:**3222–3228.
25. **Maniatis, T., J. V. Falvo, T. H. Kim, T. K. Kim, C. H. Lin, B. S. Parekh, and M. G. Wathelet.** 1998. Structure and function of the interferon-β enhanceosome, vol. LXIII. Cold Spring Harbor Laboratory Press, Cold Spring Harbor, NY.
26. **Marra, M. A., S. J. Jones, C. R. Astell, R. A. Holt, A. Brooks-Wilson, Y. S. Butterfield, J. Khattra, J. K. Asano, S. A. Barber, S. Y. Chan, A. Cloutier, S. M. Coughlin, D. Freeman, N. Girn, O. L. Griffith, S. R. Leach, M. Mayo, H. McDonald, S. B. Montgomery, P. K. Pandoh, A. S. Petrescu, A. G. Robertson, J. E. Schein, A. Siddiqui, D. E. Smailus, J. M. Stott, G. S. Yang, F. Plummer, A. Andonov, H. Artsob, N. Bastien, K. Bernard, T. F. Booth, D. Bowness, M. Czub, M. Drebot, L. Fernando, R. Flick, M. Garbutt, M. Gray, A. Grolla, S. Jones, H. Feldmann, A. Meyers, A. Kabani, Y. Li, S. Normand, U. Stroher, G. A. Tipples, S. Tyler, R. Vogrig, D. Ward, B. Watson, R. C. Brunham, M. Krajden, M. Petric, D. M. Skowronski, C. Upton, and R. L. Roper.** 2003. The genome sequence of the SARS-associated coronavirus. Science **300:**1399–1404.
27. **Mizutani, T., S. Fukushi, D. Iizuka, O. Inanami, M. Kuwabara, H. Takashima, H. Yanagawa, M. Saijo, I. Kurane, and S. Morikawa.** 2006. Inhibition of cell proliferation by SARS-CoV infection in Vero E6 cells. FEMS Immunol. Med. Microbiol. **46:**236–243.
28. **Park, S. H., J. Choi, J. I. Kang, S. Y. Choi, S. B. Hwang, J. P. Kim, and B. Y. Ahn.** 2006. Attenuated expression of interferon-induced protein kinase PKR in a simian cell devoid of type I interferons. Mol. Cell **21:**21–28.
29. **Peiris, J. S., S. T. Lai, L. L. Poon, Y. Guan, L. Y. Yam, W. Lim, J. Nicholls, W. K. Yee, W. W. Yan, M. T. Cheung, V. C. Cheng, K. H. Chan, D. N. Tsang, R. W. Yung, T. K. Ng, and K. Y. Yuen.** 2003. Coronavirus as a possible cause of severe acute respiratory syndrome. Lancet **361:**1319–1325.
30. **Prentice, E., J. McAuliffe, X. Lu, K. Subbarao, and M. R. Denison.** 2004. Identification and characterization of severe acute respiratory syndrome coronavirus replicase proteins. J. Virol. **78:**9977–9986.
31. **Rota, P. A., M. S. Oberste, S. S. Monroe, W. A. Nix, R. Campagnoli, J. P.**

Icenogle, S. Penaranda, B. Bankamp, K. Maher, M. H. Chen, S. Tong, A. Tamin, L. Lowe, M. Frace, J. L. DeRisi, Q. Chen, D. Wang, D. D. Erdman, T. C. Peret, C. Burns, T. G. Ksiazek, P. E. Rollin, A. Sanchez, S. Liffick, B. Holloway, J. Limor, K. McCaustland, M. Olsen-Rasmussen, R. Fouchier, S. Gunther, A. D. Osterhaus, C. Drosten, M. A. Pallansch, L. J. Anderson, and W. J. Bellini. 2003. Characterization of a novel coronavirus associated with severe acute respiratory syndrome. Science 300:1394–1399.

32. Sambrook, J., E. F. Fritsch, and T. Maniatis. 1989. Molecular cloning: a laboratory manual. Cold Spring Harbor Laboratory Press, Cold Spring Harbor, NY.

33. Sen, G. C. 2001. Viruses and interferons. Annu. Rev. Microbiol. 55:255–281.

34. Sims, A. C., R. S. Baric, B. Yount, S. E. Burkett, P. L. Collins, and R. J. Pickles. 2005. Severe acute respiratory syndrome coronavirus infection of human ciliated airway epithelia: role of ciliated cells in viral spread in the conducting airways of the lungs. J. Virol. 79:15511–15524.

35. Snijder, E. J., P. J. Bredenbeek, J. C. Dobbe, V. Thiel, J. Ziebuhr, L. L. Poon, Y. Guan, M. Rozanov, W. J. Spaan, and A. E. Gorbalenya. 2003. Unique and conserved features of genome and proteome of SARS-coronavirus, an early split-off from the coronavirus group 2 lineage. J. Mol. Biol. 331:991–1004.

36. Spiegel, M., A. Pichlmair, L. Martinez-Sobrido, J. Cros, A. Garcia-Sastre, O. Haller, and F. Weber. 2005. Inhibition of beta interferon induction by severe acute respiratory syndrome coronavirus suggests a two-step model for activation of interferon regulatory factor 3. J. Virol. 79:2079–2086.

37. Stark, G. R., I. M. Kerr, B. R. Williams, R. H. Silverman, and R. D. Schreiber. 1998. How cells respond to interferons. Annu. Rev. Biochem. 67:227–264.

38. Stroher, U., A. DiCaro, Y. Li, J. E. Strong, F. Aoki, F. Plummer, S. M. Jones, and H. Feldmann. 2004. Severe acute respiratory syndrome-related coronavirus is inhibited by interferon-alpha. J. Infect. Dis. 189:1164–1167.

39. Surjit, M., B. Liu, V. T. Chow, and S. K. Lal. 2006. The nucleocapsid protein of severe acute respiratory syndrome-coronavirus inhibits the activity of cyclin-cyclin-dependent kinase complex and blocks S phase progression in mammalian cells. J. Biol. Chem. 281:10669–10681.

40. Thanos, D., and T. Maniatis. 1995. Virus induction of human IFN β gene expression requires the assembly of an enhanceosome. Cell 83:1091–1100.

41. Thiel, V., K. A. Ivanov, A. Putics, T. Hertzig, B. Schelle, S. Bayer, B. Weissbrich, E. J. Snijder, H. Rabenau, H. W. Doerr, A. E. Gorbalenya, and J. Ziebuhr. 2003. Mechanisms and enzymes involved in SARS coronavirus genome expression. J. Gen. Virol. 84:2305–2315.

42. Tseng, C. T., J. Tseng, L. Perrone, M. Worthy, V. Popov, and C. J. Peters.

2005. Apical entry and release of severe acute respiratory syndrome-associated coronavirus in polarized Calu-3 lung epithelial cells. J. Virol. 79:9470–9479.

43. Vermes, I., C. Haanen, H. Steffens-Nakken, and C. Reutelingsperger. 1995. A novel assay for apoptosis. Flow cytometric detection of phosphatidylserine expression on early apoptotic cells using fluorescein labelled annexin V. J. Immunol. Methods 184:39–51.

44. Wathelet, M. G., P. M. Berr, and G. A. Huez. 1992. Regulation of gene expression by cytokines and virus in human cells lacking the type-I interferon locus. Eur. J. Biochem. 206:901–910.

45. Wathelet, M. G., C. H. Lin, B. S. Parekh, L. V. Ronco, P. M. Howley, and T. Maniatis. 1998. Virus infection induces the assembly of coordinately activated transcription factors on the IFN-beta enhancer in vivo. Mol. Cell 1:507–518.

46. Weber, F., and O. Haller. 2007. Viral suppression of the interferon system. Biochimie 89:836–842.

47. Weber, F., G. Kochs, and O. Haller. 2004. Inverse interference: how viruses fight the interferon system. Viral Immunol. 17:498–515.

48. Yang, H., C. H. Lin, G. Ma, M. Orr, M. O. Baffi, and M. G. Wathelet. 2002. Transcriptional activity of interferon regulatory factor (IRF)-3 depends on multiple protein-protein interactions. Eur. J. Biochem. 269:6142–6151.

49. Yount, B., K. M. Curtis, E. A. Fritz, L. E. Hensley, P. B. Jahrling, E. Prentice, M. R. Denison, T. W. Geisbert, and R. S. Baric. 2003. Reverse genetics with a full-length infectious cDNA of severe acute respiratory syndrome coronavirus. Proc. Natl. Acad. Sci. USA 100:12995–13000.

50. Yuan, X., J. Wu, Y. Shan, Z. Yao, B. Dong, B. Chen, Z. Zhao, S. Wang, J. Chen, and Y. Cong. 2006. SARS coronavirus 7a protein blocks cell cycle progression at G0/G1 phase via the cyclin D3/pRb pathway. Virology 346:74–85.

51. Zheng, B., M. L. He, K. L. Wong, C. T. Lum, L. L. Poon, Y. Peng, Y. Guan, M. C. Lin, and H. F. Kung. 2004. Potent inhibition of SARS-associated coronavirus (SCOV) infection and replication by type I interferons (IFN-alpha/beta) but not by type II interferon (IFN-gamma). J. Interferon Cytokine Res. 24:388–390.

52. Ziegler, T., S. Matikainen, E. Ronkko, P. Osterlund, M. Sillanpaa, J. Siren, R. Fagerlund, M. Immonen, K. Melen, and I. Julkunen. 2005. Severe acute respiratory syndrome coronavirus fails to activate cytokine-mediated innate immune responses in cultured human monocyte-derived dendritic cells. J. Virol. 79:13800–13805.